Theory of Vesicles and Droplet Type Microemulsions: Configurational Entropy, Size Distribution, and Measurable Properties

Willem K. Kegel and Howard Reiss

Department of Chemistry and Biochemistry, University of California, Los Angeles, Los Angeles CA 90024-1569, USA

Key Words: Interfaces / Microemulsions / Statistical Mechanics / Thermodynamics / Vesicles

A model of vesicles and droplet type microemulsions is presented. It is shown that the size distribution of the droplets (either vesicles or microemulsions) coexisting with excess fluid is determined in general by only two terms: the free energy of the interface between the drops and the continuous phase, and a size dependent entropic factor commonly referred to as 'the entropy of mixing'. The last mentioned term arises from translational configurations of the droplets. In this work we use an estimate of the translational contribution as derived in earlier work. A conjecture of the finite size effects coupled to the entropy of the interfacial layer is made based on experimental data.

We treat the summation over the size distribution as an 'effective partition function' from which all relevant measurable properties are calculated. The necessity of invoking a curvature dependence of the interfacial tension is proved. For vesicles, their average size is shown to scale as the volume fraction raised to a universal power, whereas their polydispersity is fully determined by a universal coefficient.

Because of the existence of a finite preferred curvature, no such universal behavior is found for microemulsions. Approximate analytical expressions for their size, interfacial tension of the planar oil-water interface, and polydispersity are obtained. A limit (though not a physical one) is found at which universal behavior is recovered.

The model is compared to experimental data found in the literature. Quantitative comparison reveals full agreement at a consistency level. Good agreement is found even when using only a single free parameter in the theory. However, this comparison points to an additional size independent term in the size distribution.

1. Introduction

Mixtures of water (with or without salt), oil and one or more surfactants may order themselves into a variety of more or less complex structures. One of the simplest possible structures are droplets of water in oil or *vice versa*, covered with a monolayer of surfactant molecules. The interfacial area is determined by the amount of surfactant, and the size of the droplets by the ratio of the dispersed volume and the interfacial area. If the surfactant concentration falls below a certain limit, part of the dispersed phase is expelled as an excess phase [1]. These kind of systems are particularly interesting as the average size of the droplets is now 'chosen' by the system, i.e. the interfacial area is fixed, but the system is free to choose the dispersed volume and the number of droplets. Moreover the interfacial tension of the planar interface between the microemulsion- and the excess phase is expected to reflect properties of the microemulsion droplets. A lot of experimental evidence exist that microemulsion droplets are polydisperse [2 – 5] and theories describing it either assume a Gaussian size distribution [6, 7] or let it follow from a free energy [8 – 10, 5]. In this work the latter approach is taken.

Vesicles are analogous to droplet type microemulsions in equilibrium with an excess phase in many ways, the most important difference being that the droplet interface consists of a bilayer instead of a monolayer. A schematic view of a microemulsion and a vesicle system is presented in Fig. 1.

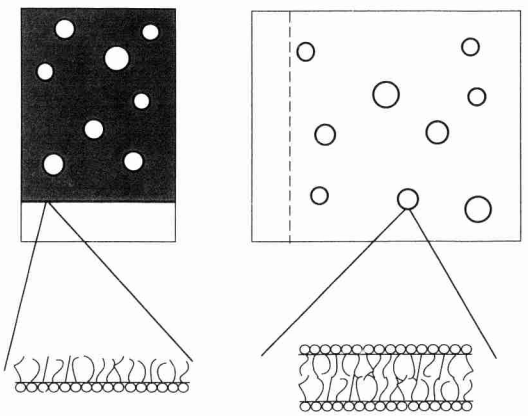

Fig. 1
Schematic representation of (left) a droplet type microemulsion coexisting with an excess phase of the same composition as the droplets (Winsor II), and (right) a system of vesicles. The dashed line represents a membrane that is permeable for all components except the surfactant

We define droplet categories j, referring to the number of surfactant molecules in a droplet, i.e. a category has a fixed average interfacial area. Every category corresponds to an average spherical shape and an average volume. The droplets are in equilibrium with a reservoir of the internal phase (i.e. in case of water droplets in oil, the system is in equilibrium with excess water). Finite size effects (due to undulations of the droplet interface and fluctuations around an average molecular area of the surfactant molecules) are taken into account by a single logarithmic term in the interfacial free energy the coefficient of which is universal and should follow from a more microscopic theory. We make a conjecture of this coefficient based on experimental data.

In Sect. 2, the free energy is calculated from the semi-exact partition function of the system. In calculating the size distribution that minimizes the free energy we follow Overbeek [11] by using the law of mass action. It is shown that this size distribution is determined by the interfacial

  0005-9021/96/0303-0300 $ 15.00+.25/0

free energy (counted as being part of the droplets), and an entropic factor which is directly related to the lengthscale associated with translational configurations of the droplets. We use an estimate for this factor made in our earlier work [12].

In Sect. 3 we proof, based on experimental information, the necessity of invoking a curvature dependence of the interfacial tension within the treatment presented here.

In Sect. 4, macroscopic, measurable properties of vesicles and microemulsions are calculated by using the size distribution as an effective partition function. For vesicles it is shown that their size depends on the volume fraction raised to a universal power that is partly determined by the length scale associated with the translational free energy. The polydispersity is fully determined by a universal coefficient.

Because of the existence of a finite preferred curvature, no such universal behavior is found for microemulsions. Approximate analytical expressions for their size, interfacial tension of the planar oil-water interface, and polydispersity are obtained. A limit (though not physical) is found where universal behavior is recovered.

The model is compared to experimental data found in the literature in Sect. 5. Although a full quantitative comparison is not possible at this stage, good agreement is found even when using only only a single free parameter in the theory. This comparison, however, points to an additional size independent term in the size distribution.

2. The Size Distribution

2.1 The free Energy of Model

In this section we derive the free energy of a system of vesicles or microemulsion droplets in equilibrium with an excess phase. The situation is as depicted in Fig. 1. The setup for the vesicle system, i.e. forcing it to be in equilibrium with 'excess' liquid at outer pressure p, may look a little awkward, but it is chosen this way in order to make the following derivation valid for both vesicle and microemulsion systems. The results are assumed to be valid also for a vesicle system without the constraint of it being in equilibrium with an excess phase, the pressure differences being only very small. This is not the case for microemulsions, as the continuous phase cannot be taken up by the droplets and *vice versa*. In the following, we refer to an 'outer phase' (subscript o) and a 'droplet phase' (subscript d). In case of vesicles, the outer phase is the same component as the bulk droplet phase; there is only a small pressure difference. For microemulsions, we consider the outer phase as 'oil' and the bulk inner phase as 'water'.

First consider the free energy of a droplet of category j, where j denotes the number of surfactant molecules in such a droplet. Gibbs [13] derived the reversible work of formation of a second phase into a bulk phase. If the Gibbs dividing surface is considered as part of the droplet, this leads to the following general expression of the Helmholtz free energy (i.e. independent of assumptions concerning the compressibily) of a droplet

$$(f_{dj})_{\text{fixed}} = \sum_i N_{ij}\mu_{ij} - p\,v_{dj} = \sum_i N_{ij}\mu^*_{ij} - (p+\Delta p_j)\,v_{dj} + \sigma_j a_j \ , \tag{2.1}$$

where N_{ij} is the number of molecules i in a droplet of category j and, because of our definition of droplet categories, $N_{sj} = j$, where the subscript 's' denotes the surfactant. μ^*_{ij} is the chemical potential of i at the pressure inside the droplet j, $p + \Delta p_j$, where p is the outer pressure and Δp_j will be related to properties of the surfactant loaded interface later. v_{dj} is the volume of a droplet j and $\sigma_j a_j$ is the interfacial free energy being interfacial tension times area of such a droplet. We have used the subscript 'fixed' for the droplet free energy as we are considering a droplet that is 'fixed in a laboratory frame' [10, 11]. As a second step, the droplets are allowed to move freely in the medium, thus releasing the 'free energy of mixing'. From now on we consider water droplets in oil, but the description is equally valid for oil in water and, of course, for vesicles. The partition function of the system may be written as

$$Q = Q_o Q_d \ , \tag{2.2}$$

where Q_o is the partition function of the outer phase,

$$Q_o = \exp\left(\frac{-1}{kT}\left(\sum_i N_{im}\mu^*_{im} - p\,V_m\right)\right) \ , \tag{2.3}$$

with k and T Boltzmann's constant and the absolute temperature, respectively, and V_m is the volume of the continuous phase. The μ^*_{im} are the chemical potentials of the components making up the outer phase at the pressure inside this phase. This pressure is raised once the droplets are allowed to move freely (and the entropy of mixing is 'switched on' which affects the chemical potential of the components in the outer phase, cf. Eq. (2.13)). Q_d is the partition function of the water droplets or vesicles (containing a surfactant layer) in the full volume V. The factorization in Eq. (2.2) is based on the idea that the interaction between oil, water and surfactant is accounted for by the interfacial free energy σA which forms part of Q_d. In case of infinitely diluted droplets

$$Q_d = \prod_j \frac{1}{n_{dj}!}(q_{dj})^{n_{dj}} \ , \tag{2.4}$$

with n_{dj} the number of droplets of category j and q_{dj} the partition function of a droplet of category j being

$$q_{dj} = q_{dj}(\text{trans}) * q_{dj}(\text{fixed}) = \frac{V}{l^3} * \exp\left[-(f_{dj})_{\text{fixed}}/kT\right] \ . \tag{2.5}$$

Where l denotes the length scale for configurational entropy that is consistent with the model. As shown in [12], this lengthscale is typically of a molecular size and is, in situations as considered in this work, virtually independent of

the thermodynamic state, i.e., among other things, of the average droplet size and the interfacial free energy. Combining Eqs. (2.1 – 2.5) using $G = F + pV = -kT\ln(Q) + pV$ leads to the Gibbs free energy

$$G = \sum_i N_{i\mathrm{m}}\mu_{i\mathrm{m}}^* + \sum_j \sum_i N_{ij}\mu_{ij}^* - \sum_j \Delta p_j V_{\mathrm{d}j} + \sum_j \sigma_j A_j + kT \sum_j n_{\mathrm{d}j}(\ln \phi_j - 1 - \ln / v_{\mathrm{d}j}/l^3)) \ , \tag{2.6}$$

where the interfacial area of all droplets of category j

$$A_j = n_{\mathrm{d}j} a_j = n_{\mathrm{d}j} 4\pi R_j^2 \ , \tag{2.7}$$

their volume

$$V_{\mathrm{d}j} = n_{\mathrm{d}j} v_{\mathrm{d}j} = n_{\mathrm{d}j} \frac{4}{3}\pi R_j^3 = \sum_i N_{ij} v_i \ , \tag{2.8}$$

with v_i the molecular volume of component i. The volume fraction of all droplets j is

$$\phi_j = \frac{4}{3}\pi R_j^3 n_{\mathrm{d}j}/V = V_{\mathrm{d}j}/\left(\sum_j V_{\mathrm{d}j} + \sum_i N_{i\mathrm{m}} v_i\right) \ . \tag{2.9}$$

Eq. (2.6) leads to the size distribution of vesicles or microemulsion drops in equilibrium with an excess phase (Fig. 1) if appropriately minimized. This is done in the next Sect. (2.2). The last term on the rhs of Eq. (2.6) defines the 'entropy of mixing' $S_{\mathrm{mix}} = -k \sum_j n_{\mathrm{d}j}(\ln \phi_j - 1 - \ln (v_{\mathrm{d}j}/l^3))$. This term takes into account the number of translational configurations of the droplets. It depends on the number of droplets of all categories and their number densities, but not on their size.

2.2 Size Distribution

In order to find the size distribution that minimizes Eq. (2.6) we follow Overbeek [10] and write the Gibbs free energy in equivalent ways as

$$G = \sum_i N_i \mu_i = \sum_i N_{i\mathrm{m}} \mu_{\mathrm{i}} + \sum_j n_{\mathrm{d}j} \mu_{\mathrm{d}j} \ . \tag{2.10}$$

By combining Eqs. (2.6) and (2.10) we get an expression for $\mu_{\mathrm{d}j}$. Then $\mu_{\mathrm{d}j}$ is eliminated using mass action. This gives the size distribution.

Now droplets of average size R_j have the properties

$$\Delta p_j = \frac{2\sigma_j}{R_j} - \frac{2c_j}{R_j^2} \tag{2.11}$$

which is the generalized Laplace equation where the bending moment

$$c_j = \left(\frac{\partial \sigma}{\partial (2/R)}\right)_{R = R_j} \ . \tag{2.12}$$

The chemical potentials of the components in the continuous medium follow from Eq. (2.6) with Eqs. (2.7 – 2.9)

$$\mu_i = \left(\frac{\partial G}{\partial N_{i\mathrm{m}}}\right)_{T,p,N_{j\mathrm{m}\neq i\mathrm{m}}} = \mu_{i\mathrm{m}}^* - kT \frac{\sum_j n_{\mathrm{d}j}}{V} v_i \ , \tag{2.13}$$

so that

$$\sum_i N_{i\mathrm{m}} \mu_i = \sum_i N_{i\mathrm{m}} \mu_i^* - kT \sum_j n_{\mathrm{d}j} \ , \tag{2.14}$$

where we have dropped a term linear in ϕ. From Eqs. (2.6) and (2.14)

$$\mu_{\mathrm{d}j} = \left(\frac{\partial G}{\partial n_{\mathrm{d}j}}\right) = \sum_i \frac{N_{ij}\mu_{ij}^*}{n_{\mathrm{d}j}} + \frac{4}{3}\pi R_j^2 \left(\sigma_j - \frac{2c_j}{R_j}\right) + kT(\ln \phi_j - \ln (v_{\mathrm{d}j}/l^3)) \ . \tag{2.15}$$

For the droplet components we have

$$\mu_{ij}^* = \mu_i' + \int_p^{p+\Delta p_j} (\partial \mu_i/\partial p)\mathrm{d}p = \mu_i' + \Delta p_j v_i = \mu_i' + \left(\frac{2\sigma_j}{R_j} - \frac{2c_j}{R_j^2}\right) v_i \ , \tag{2.16}$$

where we used Eq. (2.11). μ_i' is the chemical potential of the droplet components at pressure p. In a microemulsion (or vesicle system) coexisting with an excess phase of the same composition as the droplets we have for the droplet components

$$\mu_i' = \mu_i \ . \tag{2.17}$$

Substituting Eqs. (2.16) with (2.17) into (2.15) using, for the water components

$$\sum_i \frac{N_{ij}}{n_{\mathrm{d}j}} v_i = \frac{4}{3}\pi R_j^3 \ , \tag{2.18}$$

and writing the law of mass action as

$$\mu_{\mathrm{d}j} = \sum_i \frac{N_{ij}}{n_{\mathrm{d}j}} \mu_i \ , \tag{2.19}$$

we get the size distribution

$$\phi_j = \frac{v_{\mathrm{d}j}}{l^3} \exp(-4\pi R_j^2 \sigma_j / kT) \ . \tag{2.20}$$

It is interesting to note that the exponential factor in this expression is equal to the one obtained by Volmer as early as in 1927 [14] and by Eriksson and Ljunggren [9]. The difference between the models is reflected in different pre-exponential factors. As indicated earlier, the length l in Eq. (2.20) is typically of a molecular size. Therefore the pre-

exponential factor increases with R_j^3, while the exponential factor decreases as (neglecting for a while logarithmic contributions in the interfacial free energy) $\exp(-4\pi R_j^2\sigma_j/kT)$. In principle, this competition leads to a size distribution. However, as will be shown in the next section, in order for the size distribution to be peaked at a considerable value of R_j (say at least several nanometers as found in experiments) *and* within a physical range of the volume fraction, it is necessary either to invoke a curvature dependence of the interfacial tension or to introduce an entropic factor (with an enormous magnitude) that effectively stabilizes large drops.

We note that the length l coupled to configurational entropy was the subject of a separate study [12]. From Eq. (2.20) it is clear that its *magnitude* appears in a constant that scales the whole size distribution, while the way it depends upon the thermodynamic state defines (at least in part) the power with which R_j (in front of the exponent) rises.

3. Proof that Interfacial Tension Depends on Curvature

In this section we assume that the interfacial tension does *not* depend on curvature, and investigate the consequences of this assumption. These consequences are then compared to experimental results on microemulsions.

We take into account finite size effects coupled to undulations of the surfactant layer and fluctuations around the average molecular area of the surfactant molecules by writing

$$4\pi R_j^2\sigma_j = 4\pi R_j^2\gamma + z'kT\ln(j) \ , \tag{3.1}$$

where γ is the interfacial tension of the macroscopic oil-water interface (the planar interface between the microemulsion and the excess phase) and the second factor takes into account the finite size effects as mentioned above. It has its origin in the exclusion of long wavelength fluctuations (e.g. undulations of the monolayer or bilayer, fluctuations around the average area per surfactant molecule) due to the finite size of the microemulsion droplets or vesicles. Note that in the limit that R_j (and thus j) goes to infinity, σ_j becomes equal to γ. For several estimates of z' based on different models and assumptions is referred to [9, 15, 16]. It is found to be in the range of order ± 1. We should be careful with any comparison here as in some recent theories (see for example [16] and references therein) the coefficient is directly related to the so-called renormalization of the bending elastic moduli. We will make a conjecture for the value of z' later, using our full model. It is sufficient to note here that the calculation of z' from a model is far from trivial. For example, the problem of 'gauge fixing', which is required for such a calculation, is a very subtle matter, even for 'simple' on the average flat interfaces, as pointed out in [17].

We now derive relations between the volume fraction of droplets ϕ, the interfacial tension of the planar oil-water interface γ, and the average size of the droplets expressed by

$$R_w = \frac{\langle R^3\rangle}{\langle R^2\rangle} \ , \tag{3.2}$$

where the $\langle R^i\rangle$ represent the i-th moment of the size distribution. Combination of Eq. (2.20) with Eq. (3.1) and using that

$$4\pi R_j^2 = \sigma_s j \ , \tag{3.3}$$

in which σ_s is the molceular area of a surfactant molecule, leads to

$$\phi_j = A_1 j^z e^{-\tilde{\gamma}j} \ . \tag{3.4}$$

In this equation,

$$A_1 = \frac{4\pi}{3l^3}\left(\frac{\sigma_s}{4\pi}\right)^{3/2} \ , \tag{3.6}$$

$$\tilde{\gamma} = \gamma\sigma_s/kT \ , \tag{3.7}$$

$$z = \frac{3}{2} - z' \ . \tag{3.8}$$

The total volume fraction of the drops follows from a summation over all categories j

$$\phi = A_1 \sum_{j=1}^{\infty} j^z e^{-\tilde{\gamma}j} \ , \tag{3.9}$$

and moments of it are

$$\langle R^i\rangle = \frac{1}{\phi} A_1 \left(\frac{\sigma_s}{4\pi}\right)^{i/2} \sum_{j=1}^{\infty} j^{z+(i/2)} e^{-\tilde{\gamma}j} \ , \tag{3.10}$$

from which it is clear that ϕ acts as an effective partition function. Now iff the size distribution has its maximum at $j \gg 1$, we may replace the summations in Eqs. (3.9) and (3.10) by integrations and obtain

$$\phi \cong A_1 \int_0^{\infty} j^z e^{-\tilde{\gamma}j} dj = A_1 \Gamma(z+1)\tilde{\gamma}^{-(z+1)} \ , \tag{3.11}$$

$$\begin{aligned}\langle R^i\rangle &\cong \frac{1}{\phi} A_1 \left(\frac{\sigma_s}{4\pi}\right)^{i/2} \int_0^{\infty} j^{z+(i/2)} e^{-\tilde{\gamma}j} dj \\ &= \frac{1}{\phi} A_1 \left(\frac{\sigma_s}{4\pi}\right)^{i/2} \Gamma\left(z+1+\frac{i}{2}\right)\tilde{\gamma}^{-(z+1+i/2)} \\ &= \left(\frac{\sigma_s}{4\pi}\right)^{i/2} \frac{\Gamma(z+1+i/2)}{\Gamma(z+1)}\tilde{\gamma}^{-i/2} \ ,\end{aligned} \tag{3.12}$$

with $\Gamma(y)$ the gamma function with argument y: $\Gamma(y) = \int_0^{\infty} x^{y-1}e^{-x}dx$ which is of order 1 for y in between 1

and 4, but then increases steeply. Combining Eq. (3.12) with (3.2) leads to

$$R_w = \frac{\sqrt{(\sigma_s/\pi)}\,\Gamma(z+\frac{5}{2})}{2\Gamma(z+2)}\,\tilde{\gamma}^{-1/2}\ , \tag{3.13}$$

which clearly shows the dimensional behavior of the macroscopic interfacial tension $\gamma \sim kT/(\text{size})^2$. Writing $\tilde{\gamma}$ in Eq. (3.11) as a function of ϕ and substituting this expression into Eq. (3.13) gives

$$R_w = \chi \phi^{1/2(z+1)}\ , \tag{3.14}$$

with

$$\chi = (A_1 \Gamma(z+1))^{-1/2(z+1)} \left(\frac{2\sqrt{(\pi/\sigma_s)}\,\Gamma(z+2)}{\Gamma(z+\frac{5}{2})} \right)\ . \tag{3.15}$$

We will now compare the model described above to experimental results. First, it follows from experiments (see e.g. [5, 11, 18, 19]) that a typical set of values for the volume fraction, average droplet radius (R_w is actually obtained from the amount of water and the amount of surfactant in the microemulsion phase) and the interfacial tension are $\phi = 0.05$, $R_w = 2-10$ nm, $\gamma = 0.001-0.1$ mN/m. Can these values be recovered to the same order of magnitude by using Eqs. (3.4) and (3.10)? We require $\phi = 0.05$ and vary γ in such a way that this requirement is fulfilled. This leads to $\gamma = 15$ mN/m and droplets of typically a molecular size ($R_w = 0.28$ nm when using $l = 0.1$ nm) for $z = 3/2$; even a larger interfacial tension and smaller 'droplets' if z is decreased, and only values in the neighborhood of the experimental ones for $z > 25$. Even when $z = 25$, $\gamma = 4$ mN/m and $R_w = 1.4$ nm. On the other hand, if we lift the constraint of a physical volume fraction, we get R_w of order 1 nm and γ of order 0.1 mN/m, but only with $\phi \gg 1$. A second consequence of the assumption that the interfacial tension does not depend on curvature is the prediction that R_w grows with ϕ raised to a universal power, Eq. (3.14). Therefore, plotting $\ln R_w$ versus $\ln \phi$ should lead to a system independent slope with a value smaller than $1/2(z+1) = 1/52$. Fig. 2 shows $\ln R_w$ versus $\ln \phi$ of 3 different systems.

It is clear from Fig. 2 that the slopes are not universal, and not smaller than 1/52 (they correspond, going from the upper to the lower curve, to $z = 1.5$, 5.2, and 6.6, respectively). We will return to this figure in the next section. This analysis shows that the model presented in this section clearly fails to explain the experimental data shown in Fig. 2.

Summarizing this section, the stability of large droplets (say several nm in size) with a positive interfacial tension may be explained in two ways. First, there could be a factor coupled to configurational or interfacial entropy that effectively stabilizes large droplets (explicit in the value of z), and second, there may be a preferred curvature with an associated stiffness that prevents the droplets from shrinking down to a molecular size. The results of this section rules out the first possibility. If it were true, a universal slope in Fig. 2 would have been found that corresponds to $z > 25$ (see Eq. (3.14)). Instead, the experimental results shown in Fig. 2 show a significantly varying slope that corresponds to values of z in between 3/2 and 6.6. Therefore, if there was not interfacial tension penalty upon shrinking the droplets, microemulsions and vesicles cannot be stable. In other words: in that case the system would maximize its entropy associated with translational configurations by forming many droplets.

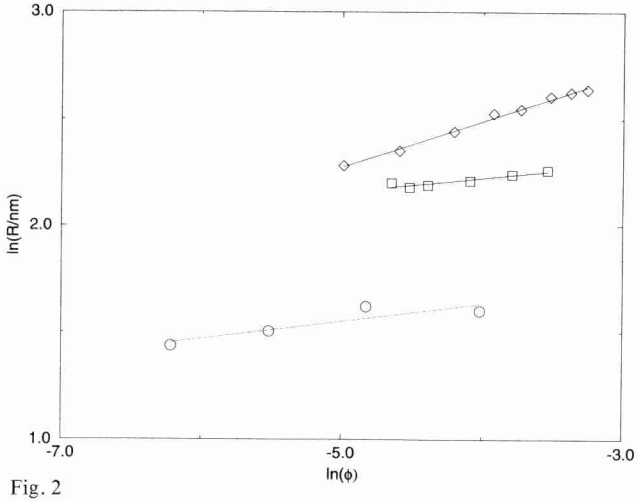

Fig. 2
Log-log plot of experimentally determined average droplet size versus volume fraction. The upper set of data are from [5] and correspond to a system composed of SDS (Sodium dodecyl Sulfate), pentanol, cyclohexane, and 0.2 M NaCl (Sample series II in [5]). The SDS concentration and the pentanol concentration necessary to compensate for the uptake in the monolayers was varied in this system. The middle set was obtained from [19] and is essentially the same system as above except for a somewhat higher pentanol concentration. The lower set is from [30] and correspond to a system composed of deuterated water, AOT and deuterated n-decane at emulsification failure. The apparent values of z (as defined in the text) are 3/2, 5.2 and 6.6, respectively

The only way to understand why R_w apparently grows with ϕ in a manner that depends on the system, is to assume that the systems shown in Fig. 2 all have different preferred curvatures with an associated stiffness. This statement will be made more quantitative in the next section.

4. Size Distribution and Measurable Properties of Vesicles and Microemulsions

4.1 General Expression for the Size Distribution

Since experiments indicate that 'large' droplets are not stabilized by an entropic factor, we now take into account the curvature dependence of the interfacial tension. The interfacial tension is easily related to Helfrich's [20] curvature free energy, which, for a sphere, reads

$$\mathrm{d}F_c = \left(2K\left(\frac{1}{R} - c_0\right)^2 + \bar{K}/R^2 \right)\mathrm{d}A\ , \tag{4.1}$$

where K is the bending elastic modulus, c_0 the preferred curvature, and $\bar{K}$ denotes the modulus associated with Gaussian curvature. This expression allows us to relate the interfacial tension of the droplets to the macroscopic interfacial tension between the microemulsion (or vesicle system) and the excess liquid phase, γ (which is measurable in case of microemulsions; in vesicle systems such an interface is simply not present)

$$\begin{aligned}\sigma &= \gamma + \int_0^{2/R} \left(\frac{\partial \sigma}{\partial (2/R)}\right) \mathrm{d}(2/R) + z' k T \ln(j)/4\pi R^2 \\ &= \gamma + \int_0^{2/R} \left(\frac{\partial^2 F_c}{\partial A\, \partial (2/R)}\right) \mathrm{d}(2/R) + z' k T \ln(j)/4\pi R^2 \\ &= \gamma + \frac{(2K+\bar{K})}{R^2} - \frac{4Kc_0}{R} + z' k T \ln(j)/4\pi R^2 \ . \end{aligned} \tag{4.2}$$

Combining Eq. (4.2) with Eqs. (2.20) and (3.3) we find the size distribution

$$\phi_j = A_2 j^z \mathrm{e}^{\tilde{c}_0 j^{1/2}} \mathrm{e}^{-\tilde{\gamma} j} \ , \tag{4.3}$$

with

$$A_2 = \frac{4\pi}{3l^3} \left(\frac{\sigma_s}{4\pi}\right)^{3/2} \exp\left(\frac{-4\pi(2K+\bar{K})}{kT}\right) \ , \tag{4.4}$$

and

$$\tilde{c}_0 = \frac{16\pi K c_0}{kT} \left(\frac{\sigma_s}{4\pi}\right)^{1/2} \ . \tag{4.5}$$

The size distribution Eq. (4.3) with (4.4 – 4.5) is plotted for 3 different values of γ corresponding to 3 different surfactant concentrations where $c_0 = 0$ and $c_0 = 0.05$, and $z = 3/2$ and $z = 1.0$ are used (it will be shown later that z is indeed, roughly, in this range). Since vesicles consist of bilayers instead of monolayers, vesicle categories are distinguished by different numbers of surfactant *pairs* instead of single surfactant molecules. The surfactant concentrations were calculated via

$$c_s = \frac{N_s}{V} = \sum_{j=1}^{\infty} \frac{j n_{dj}}{V} = \sum_{j=1}^{\infty} \frac{j\phi_j}{v_{dj}} \ , \tag{4.6}$$

where N_s denotes the number of surfactant molecules at the droplet interface in case of microemulsions, and the number of surfactant pairs in case of vesicles. A more convenient expression for c_s will be derived later.

In ending this section we note that perturbation methods and renormalization group theory on tensionless surfaces without preferred curvature predict that the bending elastic moduli logarithmically vary with j [21 – 23]. This renormalization effectively accounts for surface entropy coupled to thermal undulations. In the treatment presented here, most of the interfacial entropy is already accounted for by the macroscopic interfacial tension γ. Therefore, taking into account an additional size dependency of the bending elastic moduli would introduce redundancies in the interfacial entropy.

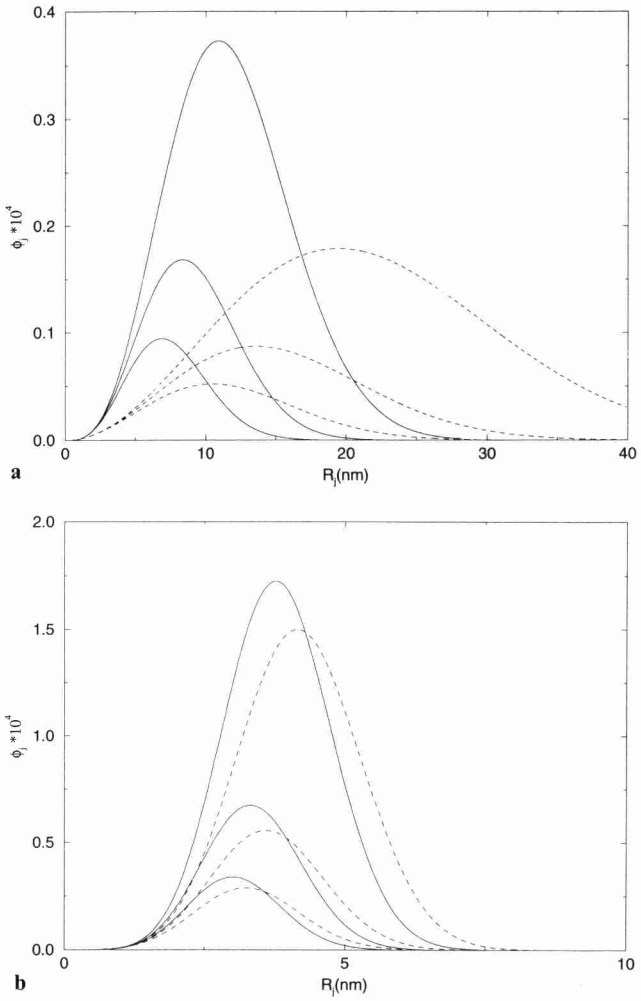

Fig. 3
Size distributions calculated with Eq. (4.3 – 4.5) in the $\phi_j - R_j$ plane for $c_0 = 0$ (Fig. 3a) and $c_0 = 0.05\ \mathrm{nm}^{-1}$ (Fig. 3b). The solid curves were calculated using $z = 3/2$, while for the dashed ones $z = 1$ was used. Going from the upper to the lower curve, the surfactant concentration was fixed at 0.03, 0.01 and 0.005 nm^{-3}, respectively. For all size distributions we used $l^3 = 0.1\ \mathrm{nm}^3$ $\sigma_s = 1\ \mathrm{nm}^2$, $K = kT$, and $\bar{K} = -kT/2$

4.2 Vesicles

In the case of vesicles we assume $\tilde{c}_0 = 0$. This is probably a good approximation for relatively large vesicles so that concentration- and pressure differences between the inside and the outside become negligible. Eq. (4.3) then becomes

$$\phi_j = A_2 j^z \mathrm{e}^{-\tilde{\gamma} j} \ , \tag{4.7}$$

with A_2 given by Eq. (4.4). Interestingly, preferred curvature does not appear explicitly here, but the presence of the bending elastic moduli in Eq. (4.7) (via Eq. (4.4)) being of order kT provide a 'weighting factor' for the whole set of $\{\phi_j\}$ that leads to $\phi \ll 1$ where otherwise one would have found $\phi \gg 1$. It leads to size distributions corresponding to slightly positive interfacial tensions and still with sizes of order 10 nm, see Fig. 3a. The absence of the preferred curvature in Eq. (4.7) leads to several intriguing results.

We calculate the volume fraction and R_w in the same way as in the previous section (i.e. by replacing the summation over the ϕ_j by an integration) and find

$$\tilde{\gamma} = \chi_1 \phi^{-1/(z+1)} = \chi_2 R_w^{-2} \ , \tag{4.8}$$

with

$$\chi_1 = \sigma_s^{-1} (A_2 \Gamma(z+1))^{1/(z+1)}$$

$$\chi_2 = \left(\frac{\Gamma(z+\frac{5}{2})}{2\sqrt{(\pi/\sigma_s)}\,\Gamma(z+2)} \right)^2 \ , \tag{4.9}$$

showing that the interfacial tension of a planar bilayer, if such layer was present, is finite and depends upon the thermodynamic state! From Eq. (4.8) we find how the average size of the vesicles grows with the volume fraction

$$R_w = \chi \phi^{1/2(z+1)} \tag{4.10}$$

which is analogous to Eq. (3.14), but now with the proportionality factor given by

$$\chi = (A_2 \Gamma(z+1))^{-1/2(z+1)} \left(\frac{2\sqrt{(\pi/\sigma_s)}\,\Gamma(z+2)}{\Gamma(z+\frac{5}{2})} \right) \ . \tag{4.11}$$

So in case of vesicles, the theory clearly predicts that the average size grows with the volume fraction raised to a universal power. Such a result was also found by Simons and Cates [24] using an *ansatz* for the grand potential that consists of the sum of the (renormalized) curvature free energy, Eq. (4.1) but with size dependent bending elastic moduli, and some 'entropy of mixing'. Clearly their chemical potential μ/kT of the surfactant is completely analogous to our interfacial tension $\tilde{\gamma}$.

Another interesting quantity is the polydispersity defined by

$$\sigma^2 = \frac{\langle R^2 \rangle}{\langle R \rangle^2} - 1 \ , \tag{4.12}$$

which can be calculated by again using the volume fraction as a partition function (as in Eq. (3.12))

$$\sigma^2 + 1 = \frac{\frac{1}{\phi} A_2 (\sigma_s/4\pi) \int_0^\infty j^{z+1} e^{-\tilde{\gamma} j} dj}{\left(\frac{1}{\phi} A_2 (\sigma_s/4\pi)^{1/2} \int_0^\infty j^{z+(i/2)} e^{-\tilde{\gamma} j} dj \right)^2}$$

$$= \frac{\Gamma(z+1)\Gamma(z+2)}{\Gamma^2(z+3/2)} \ , \tag{4.13}$$

where we have used the relation between the macroscopic interfacial tension and the volume fraction, Eq. (4.8) with (4.9). Eq. (4.13) shows the very interesting (and new) result that the polydispersity of vesicles only depends upon a universal coefficient. It is independent of the bending elastic moduli, the macroscopic interfacial tension and the volume fraction. So although it is necessary to introduce bending elastic moduli in order to explain the stability of vesicles, the polydispersity doesn't depend on them and nor does the coefficient that determines how their size grows with the volume fraction.

4.3 Microemulsions

In this section, we study how measurable properties of microemulsions are interrelated. First we show that a finite preferred curvature breaks down the universal behavior as discovered in the previous section. In the second part we derive approximate analytical solutions for the quantities of interest in Winsor II microemulsions. We show that a limit (though unphysical) exists where this behavior is recovered.

As a general purpose, we substitute $x = j^{1/2}$ in Eq. (4.3), and obtain for the total volume fraction, replacing the summation by an integration

$$\phi = 2A_2 \int_0^\infty x^{2z+1} e^{\tilde{c}_0 x} e^{-\tilde{\gamma} x^2} dx \ . \tag{4.14}$$

Now in order to study how a finite preferred curvature influences the quantities mentioned above relative to the situation with zero preferred curvature, we expand the exponent of the preferred curvature in Eq. (4.14) and find

$$\phi/2A_2 = \int_0^\infty x^{2z+1} \left(\sum_{i=0}^\infty \frac{(\tilde{c}_0 x)^i}{i!} \right) e^{-\tilde{\gamma} x^2} dx$$

$$= \sum_{i=0}^\infty \left(\frac{(\tilde{c}_0)^i}{i!} \int_0^\infty x^{2z+1+i} e^{-\tilde{\gamma} x^2} dx \right)$$

$$= \sum_{i=0}^\infty \left(\frac{\tilde{c}_0^i}{i!} \right) \Gamma(z+1+i/2)\, \tilde{\gamma}^{-(z+1+i/2)} \ . \tag{4.15}$$

Because of the separation of universal and non-universal quantities, Eq. (4.15) clearly describes how the 'partition function' $\phi(\tilde{\gamma})$ starts deviating from universal behavior. Since R_w still goes to leading order as Eq. (4.8), we get

$$\phi \sim \sum_{i=0}^\infty \left(\frac{\tilde{c}_0^i}{i!} \right) \Gamma(z+1+1/2) R_w^{2(z+1)+i} \ . \tag{4.16}$$

This equation shows that if c_0 increases, $\phi(R_w)$ increases faster and therefore $R_w(\phi)$ starts leveling off. How does this relate to experimental results? The upper two lines in Fig. (2) correspond to systems in which the preferred curvature is significantly different (i.e. the systems are equal except for the cosurfactant concentration which alters c_0) and the lower one of the two has the largest preferred cur-

vature. Clearly its slope is smaller which is indeed in agreement with the trend inferred from Eq. (4.16). We will return to a more quantitative interpretation of these data in the next section.

An approximate analytical solution of Eq. (4.14) is obtained by using a saddle point method known as steepest descent. This leads to

$$\phi = A_2 e^{f(x^*)} \sqrt{(\pi/\tilde{\gamma})}\,(1+\mathrm{Erf}\,(u/2\sqrt{\tilde{\gamma}})) + (\text{slowly varying functions of } \tilde{c}_0 \text{ and } \tilde{\gamma})\ , \tag{4.17}$$

where we will further neglect the slowly varying functions of $\tilde{c}_0$ and $\tilde{\gamma}$. In this equation,

$$f(x^*) = -\tilde{\gamma}(x^*)^2 + \tilde{c}_0 x^* + (2z+1)\ln(x^*)\ , \tag{4.18}$$

in which x^* is the value of x where the size distribution has its maximum

$$x^* = (\tilde{c}_0 + (\tilde{c}_0 + 8\tilde{\gamma}(2z+1))^{1/2})/4\tilde{\gamma}\ , \tag{4.19}$$

and

$$u = 2\tilde{\gamma}x^*\ . \tag{4.20}$$

(Note the importance of the macroscopic interfacial tension in determining the peak in the size distribution!). In the case that $\tilde{c}_0 > 0$ (even very slightly), the error function in Eq. (4.17) equals 1 so that

$$\phi \cong 2\sqrt{\pi} A_2 e^{f(x^*)} \tilde{\gamma}^{-1/2}\ . \tag{4.21}$$

In the same way as in Sect. 3, the i-th moments of the average globule size of a microemulsion system is found to be

$$\langle R^i \rangle = \frac{2\sqrt{\pi} A_2}{\phi}\left(\frac{\sigma_s}{4\pi}\right)^{i/2} e^{-f(x_i^*)}\tilde{\gamma}^{-1/2} = \left(\frac{\sigma_s}{4\pi}\right)^{i/2} \exp\left(f(x^*) - f(x_i^*)\right)\ , \tag{4.22}$$

with

$$f(x_i^*) = -\tilde{\gamma}(x_i^*)^2 + \tilde{c}_0 x_i^* + (2z+1+i)\ln(x_i^*)\ , \tag{4.23}$$

and

$$x_i^* = (\tilde{c}_0 + (\tilde{c}_0^2 + 8\tilde{\gamma}(2z+1+i))^{1/2})/4\tilde{\gamma}\ . \tag{4.24}$$

The only conserved quantity in the microemulsion phase is (to a very good approximation) the surfactant concentration, which can be obtained by starting with Eq. (4.6) and making use of the results above, leading to

$$c_s = A_3 e^{f(x_2^*)} \tilde{\gamma}^{-1/2} \tag{4.25}$$

with

$$A_3 = \frac{2\sqrt{\pi}\exp(-4\pi(2K+\bar{K})/kT)}{l^3}\ , \tag{4.26}$$

$$f(x_2^*) = -\tilde{\gamma}(x_2^*)^2 + \tilde{c}_0 x_2^* + 2z\ln(x_2^*)\ , \tag{4.27}$$

$$x_2^* = (\tilde{c}_0 + (\tilde{c}_0 + 16z\tilde{\gamma})^{1/2})/4\tilde{\gamma}\ . \tag{4.28}$$

The approximate expressions above were all checked by numerical integrations and the agreement was always better than 1% difference.

4.4 Model Predictions

In Fig. 4a, b, and d we plot the macroscopic interfacial tension, the average globule size R_w, and the polydispersity as a function of the volume fraction for several values of c_0 and fixed $z = 3/2$, K and $\bar{K}$, respectively. Fig. 4c shows the logarithm of R_w against the logarithm of ϕ. The value of z does not influence the trends shown in these figures. Although the interfacial tension slightly decreases with the volume fraction for all values of c_0 (Fig. 4a), it is clear from Fig. 4b that a significant (and measurable) increase of the average droplet radius can only be obtained as long as the preferred curvature is not too far from zero (at least for the used values of the other parameters). Fig. 4c shows how the apparent scaling coefficient decreases with the preferred curvature, as predicted by Eq. (4.16). In Fig. (4d), all polydispersities go to the value corresponding to the vesicle case when ϕ approaches zero. So, interestingly, at very small volume fractions, universal behavior is recovered. This can be understood as follows. For very small volume-fractions, the value of x where the size distribution has its maximum is much smaller than $1/c_0$, so that we may replace the upper integration limit in Eq. (4.14) by x_{max} with x_{max} such that $c_0 x \ll 1$ over the whole integration from 0 to x_{max}. This allows us to put the exponential term with c_0 equal to one, and the results for the situation where $c_0 = 0$ (vesicles) is recovered. Although the values of ϕ where this behavior is observed are unphysical (in the sence that we don't expect a 'microemulsion' any more but at most micelles and even more probable monomers of surfactant molecules), this result is interesting as it illustrates the connection between vesicles and microemulsion droplets: 'microemulsions lose their identity as their volume fraction goes to zero' in the theory presented here.

From Fig. 4d it is clear that in the cases where $\tilde{c}_0 \neq 0$, the polydispersity decreases with the volume fraction of the droplets. This trend has indeed recently been observed in microemulsions made of nonionic surfactants [25]. It follows from Fig. 4d that it also decreases with c_0. The fact that the polydispersity is constant for the vesicle case implies that the decrease in polydispersity as a function of ϕ as observed in the microemulsions cannot simply be explained by a competition between mixing entropy and bending energy *in general*. It rather is a consequence of the fact that the *shape* of the size distribution changes with ϕ due to

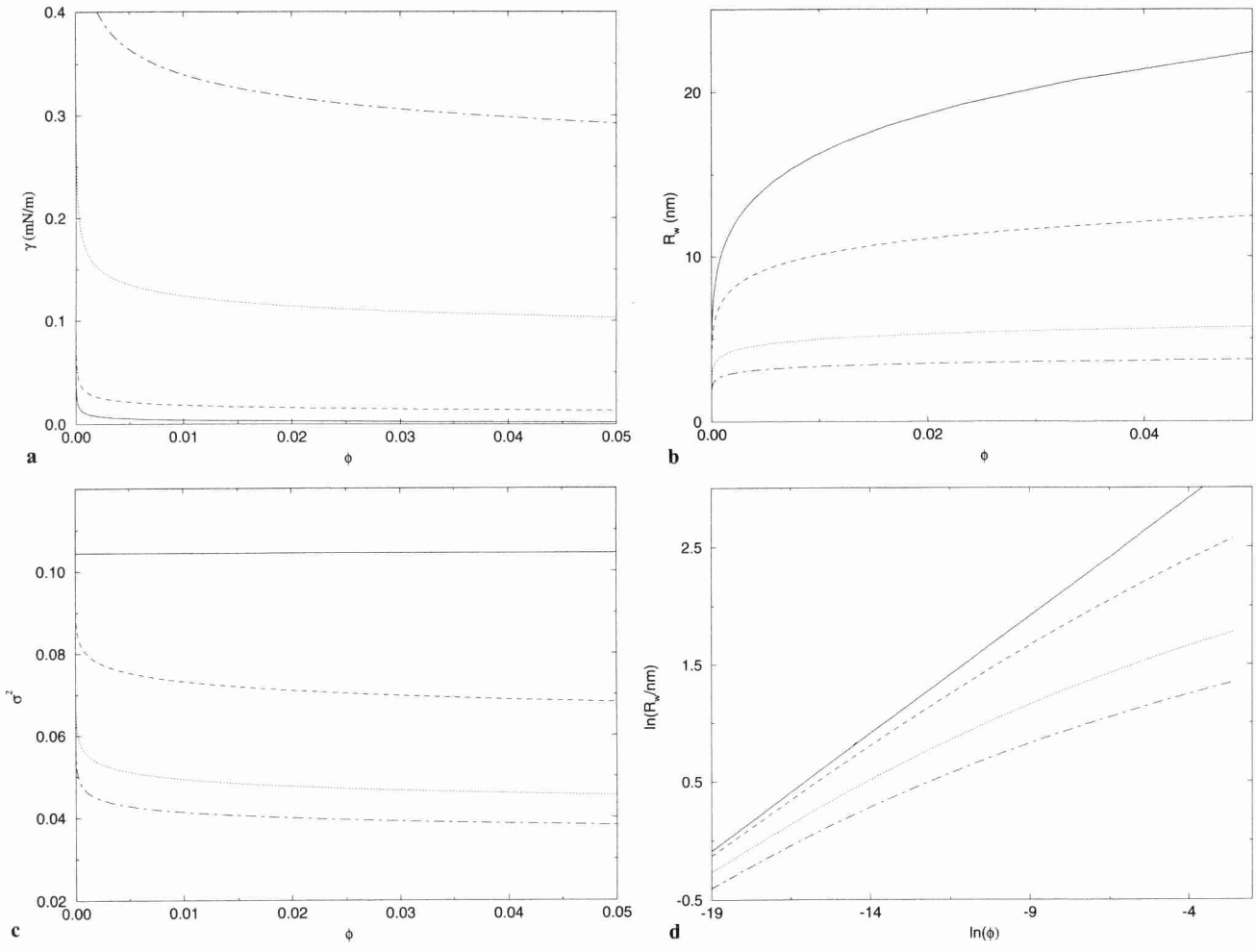

Fig. 4

a) Interfacial tension of the planar interface γ versus the volume fraction of the droplets ϕ with fixed values of $\ell^3 = 0.1\ \mathrm{nm}^3$, $\sigma_s = 1\ \mathrm{nm}^2$, $K = kT$ and $\bar{K} = -kT/2$. Different values of c_0 (in nm^{-1}) were used: $c_0 = 0$ (Eq. (4.8); solid line), $c_0 = 0.01$ (dashed line), $c_0 = 0.05$ (dotted line), and $c_0 = 0.10$ (dash-dotted line)

b) Squared polydispersities σ^2 as a function of the droplet volume fraction. Parameters and line symbols as in Fig. 4a

c) Droplet radius R_w as a function of the droplet volume fraction. Parameters and line symbols as in Fig. 4a

d) As Fig. 4c, but now in the log-log plane for the purpose of demonstrating how preferred curvature influences the apparent scaling of the average droplet size with volume fraction

the interplay of two functions (a power and an exponential) that increase with j. So in that respect, it indeed is an interplay between mixing entropy and interfacial free energy, but only that part of the interfacial free energy that contains the preferred curvature and its associated stiffness is involved in this interplay.

5. Comparison with Experiments

5.1 Conjecture of the Finite Size Effect

The slopes in Fig. 2 are $1/2(1+z_{app})$, with z_{app} the apparent value of z which is determined mainly by z and $\tilde{c}_0$. This becomes clear when looking at Fig. 4c where it is shown that the slope of $\ln(R_w)$ versus $\ln(\phi)$ clearly decreases with $\tilde{c}_0$ if z is kept constant. Quantitatively, this is most clear from Eq. (4.15). Now first we verify that it is indeed $\tilde{c}_0$ that increases in these systems when going from the upper to the lower line in Fig. 2.

$\tilde{c}_0$ depends on both K and c_0, see Eq. (4.5), and only slightly on σ_s which does not vary very much per system anyway. Since K of all these systems is approximately equal to kT [5, 26], where it is assumed that deuteration of water and oil does not significantly influence the value of K, the systems with smaller (average) R_w should have a larger preferred curvature. Therefore the lower the lines in Fig. 2, the smaller their slope and therefore the larger their z_{app} should be. This is indeed (and significantly) observed (it is even immediately clear that the system with more pentanol should have a larger c_0, which is therefore consistent with the reasoning above).

We immediately obtain an upper limit for z from the slopes in Fig. 2. Since in these systems $\tilde{c}_0 > 0$, and, as proved before, in that case $z_{app} > z$, and the smallest value of

z_{app} we get from Fig. 2 is $z_{app} \approx 3/2$, we immediately find $z < 3/2$. This implies that the coefficient related to the finite size effects $z' > 0$.

To obtain a lower bound is a little bit less straightforward. Using the results of Sect. 4.3 with varying z, c_0 and bending elastic moduli we found that R_w is always much smaller than $1/c_0$. In order to remain at the save side, we assume for the radii in Fig. 2 $R_w \leq 1/2c_0$. Comparing the slopes generated using the value of $c_0 = 1/2R_w$ (as in Fig. (4c)), we estimate $z > 3/4$. This leads to our conjecture of z based on experimental input

$$3/4 < z < 3/2 \ , \tag{5.1}$$

so that $0 < z' < 3/4$. Experimentally, a more accurate value of z can only be obtained by measuring some average radius versus the volume fraction in a thermodynamically stable vesicle system. Even then one has to be careful as very small concentration differences between the inside and the outside liquid or between the inner- and outer part of the surfactant bilayer may lead to a significantly non-zero preferred curvature.

Ultimately, z' should follow from a theoretical model of fluctuating bilayers and monolayers. At present, there is no such model that is able to come up with a value of z' in the range corresponding to Eq. (5.1).

5.2 Average Droplet Size and Macroscopic Interfacial Tension as a Function of Droplet Volume Fraction

Experimental evidence that the average size of microemulsion droplets and the macroscopic interfacial tension depend on the droplet volume fraction was, for the first time, shown by van Aken [19] (his data are also published in [5]). Since the bending elastic modulus of this system is known [5], the results of Sect. 4.3 imply that there are still two unknown constants, the Gaussian bending elastic modulus and the preferred curvature, in the theory. Therefore we choose to test the theory on consistency, i.e. we fix z, fit the (R_w, ϕ) data with Eqs. (4.21 – 4.24), and subsequently compare the values of the interfacial tension that were necessary to generate these data with the experimental values. Note that the last mentioned comparison requires no adjustable parameters. Fig. 5a shows some 'fitresults' of the average droplet size versus the volume fraction for $z = 3/2$, and Fig. 5b shows the set of values of the interfacial tension that were used to generate these curves.

We note that the agreement is excellent. Comparable agreement is found over the whole range of z as given by Eq. (5.1). The value of c_0 obtained in this way increases somewhat with z, and the value of $\bar{K}$ decreases. The signs of both c_0 and $\bar{K}$ are intuitively sound: the preferred curvature should have the same sign as the droplet radius whereas $\bar{K}$ is the negative second moment of the lateral pressure profile [27] and is expected to be negative.

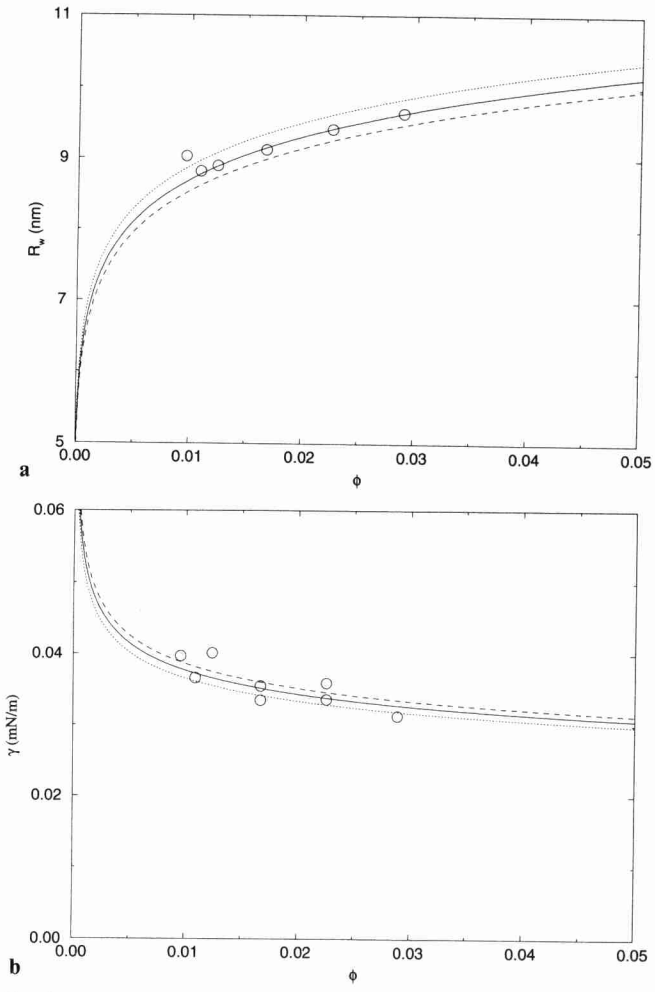

Fig. 5
Experimental data of van Aken [19] together with theoretical lines calculated from Eqs. (4.21 – 4.24) using $K = kT$ [5], $\ell^3 = 0.1\,\text{nm}^3$, $\sigma_s = 1\,\text{nm}^2$, $z = 3/2$, $c_0 = 0.025\,\text{nm}^{-1}$, and $\bar{K}/kT = -0.07$ (dotted line), -0.09 (solid line), and -0.10 (dashed line). The $R_w(\phi)$ data in Fig. 5a were 'fitted' using c_0 and $\bar{K}$ as free parameters. The variation of the macroscopic interfacial tension γ necessary to produce the lines in Fig. (5a) are plotted in Fig. (5b), together with the experimental points. There is no additional free parameter. Smaller values of z in the range of Eq. (5.1) give comparable results, only slightly larger c_0 (up to a factor 2) and more negative $\bar{K}$ (down to approximately $-kT$)

5.3 The Macroscopic Interfacial Tension as a Function of the Salt Concentration

The interfacial tension as a function of the salt concentration for systems composed of AOT (sodium diethylhexylsulphosuccinate), brine and linear alkanes of varying chainlength (C8, C10, C12 and C14) was presented by Binks et al. [26]. In this work, the bending elastic moduli are determined as well. In order to describe how the interfacial tension varies with the salt concentration using the model in the work presented here, we need to know how K, $\bar{K}$, and c_0 vary with the salt concentration. These parameters (or at least certain linear combinations of them) are in fact moments of the lateral pressure profile [27] which, in case of ionic surfactant systems, is in turn the sum of the lateral

pressure profile due to the hydrocarbon chains and the one due to the electrical double layer. The first one cannot be obtained analytically [28], but the second was found using the full (non-linear) Poisson-Boltzmann equation [29]. It turns out that the influence of the salt concentration on the bending elastic moduli is negligible in the salt concentration range that is of interest here, but it significantly influences the linear combination

$$(Kc_0)_{el} = -\frac{kT}{\pi Q}\ln((q+1)/2) \ , \tag{5.2}$$

where the subscript 'el' refers to the contribution of the electrical double layer. Contrary to [29] a minus sign is used here because of our definition of c_0 (it should have the same sign as the droplet radius). Q is the Bjerrum length being 0.714 nm in aqueous systems at $T = 298$ K and

$$q = (p^2+1)^{1/2} \ ; \quad p = 2\pi Q\sigma/\kappa e \ , \tag{5.3}$$

in which σ denotes the absolute surface charge density, κ the inverse Debye length ($\kappa \simeq 3.3(c_{salt})^{1/2}$ with c_{salt} in mol/l and κ in nm^{-1} for a 1:1 electrolyte at 298 K), and e the unit charge. The surface charge density is related to the (ionic) surfactant molecular area (reported in [18]) via $\sigma = e/\sigma_s$. So, to a good approximation we may write the preferred curvature as

$$c_0 = \frac{(c_0K)_{chain} + (c_0K)_{el}}{K} \ , \tag{5.4}$$

where the subscript 'chain' refers to the contribution of the surfactant chains. The interfacial tension as reported in [26] as a function of the salt concentration first decreases, goes to a minimum and then increases. $(Kc_0)_{chain}$ can now be obtained from the salt concentration where the interfacial tension has a minimum since in that case it is expected that $c_0 = 0$ and thus $-(Kc_0)_{chain} = (Kc_0)_{el}$ is given by Eq. (5.2) at this salt concentration. Now $(Kc_0)_{chain}$ may vary with the salt concentration as well due to some variation of the packing density of the surfactant molecules in the monolayers with the salt concentration. This effect, if present, is at least very small as no significant variation of the surfactant molecular area was found in the salt concentration range where the experiments reported in [26] were performed [18], so we will neglect it here. This fixes all model parameters except one, $\bar{K}$.

The surfactant concentration in the systems mentioned above is conserved and therefore we use Eqs. (4.25 – 4.28) to obtain a relation betwen the macroscopic interfacial tension and the salt concentration. We may set $(\tilde{c}_0/\tilde{\gamma}) \gg 1$ in these systems (which is verified afterwards) to obtain

$$x_2^* \cong \frac{\tilde{c}_0}{2\tilde{\gamma}} + \frac{2z}{\tilde{c}_0} \ , \tag{5.5}$$

substituting this equation into Eqs. (4.27) and (4.25) and taking the logarithm on both sides we get

$$a(\tilde{\gamma})\tilde{c}_0^4 - b(\tilde{\gamma}, \tilde{c}_0, z, c_s, A_3)\tilde{c}_0^2 - c(\tilde{\gamma}, z) = 0 \ , \tag{5.6}$$

with

$$a(\tilde{\gamma}) = 1/4\tilde{\gamma} \ , \tag{5.7}$$

$$b(\tilde{\gamma}, \tilde{c}_0, z, c_s, A_3) = \ln(c_s) - \ln(A_3) + \frac{1}{2}\ln(\tilde{\gamma}) - 2z\ln\left(\frac{\tilde{c}_0}{2\tilde{\gamma}} + \frac{2z}{\tilde{c}_0}\right) \ , \tag{5.8}$$

and

$$c(\tilde{\gamma}, z) = 4z^2\tilde{\gamma} \ . \tag{5.9}$$

Eq. (5.6) was solved numerically and combined with Eqs. (5.2) to (5.5) to obtain (real and positive) pairs of $(\tilde{\gamma}, c_{salt})$. The results together with the experimental data are shown in Fig. 6. The fixed parameters that were used to calculate these curves are summarized in Table 1. Varying z between the limits Eq. (5.1) did not have any visible influence on the theoretical lines in Fig. 6.

Table 1
Fixed parameters obtained from Ref. [26] and [18] used to calculate the dependence of the interfacial tension on the salt concentration. A surfactant concentration of 7.5 mM in the microemulsion phase was used in all cases [26]; $z = 3/2$; $\ell^3 = 0.1$ nm^3

System (oil phase)	K/kT	$(Kc_0)_{chain}/kT\,nm^{-1}$	σ_s/nm^2
Octane (C8)	0.85	0.744	0.71
Decane (C10)	0.95	0.633	0.67
Dodecane (C12)	0.15	0.489	0.64

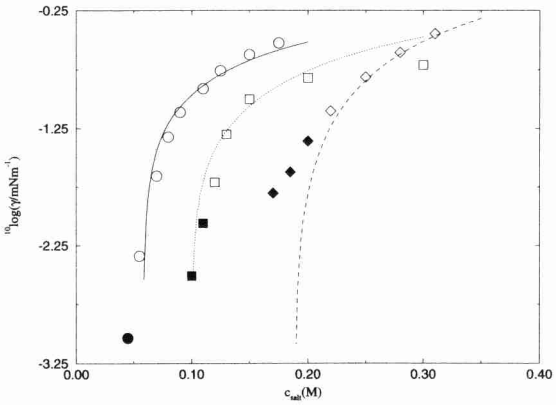

Fig. 6
Interfacial tension of the planar interface between the microemulsion and the excess phase as a function of the salt concentration for systems composed of AOT (sodium diethylhexylsulphosuccinate), brine and linear alkanes of varying chainlength. Points are experimental data obtained from [26]: C8 (circles), C10 (squares), and C12 (diamonds). Open symbols refer to Winsor II systems, while the corresponding filled symbols indicate the Winsor III region, where the theory is no longer valid. The lines were calculated using Eqs. (5.2 – 5.9), the fixed parameters listed in Table 1, and well chosen values of $\bar{K}/kT = 1.0$ (dodecane system), 1.9 (decane system), and 4.0 (octane system)

The theoretical lines in Fig. 6 correspond to well chosen values of $\bar{K}$. Other values only translate the curves through the $(\tilde{\gamma}, c_{\text{salt}})$ plane without altering their shapes. It is emphasized that these curves are all unique. For example, there exist no values of $\bar{K}$ that allows the C10 or the C12 data to be described by the parameters corresponding to the C8 data.

It is clear from Fig. 6 that all the relevant experimental data are described very well by the theory. A worrysome result is, however, the positive value of $\bar{K}$ that is found. There are roughly two possibilities that might explain this counter-intuitive result.

First, is was shown experimentally [26] that the phase behavior of these systems is very different from the 'classical' behavior as found by Winsor [1], i.e., as the middle phase is reached, the systems form structures that consist of bilayers instead of monolayers. Therefore there should be an attractive potential between the chain sides of the monolayers that is not present (or to a smaller extend) in other systems. This attractive potential should then also be present between chains that are part of the same monolayer and this may reduce the contribution of the chains to the lateral pressure profile of the monolayers, which will cause $\bar{K}$ to become at least less negative compared to a system where such attraction is not present. It is however questionable whether this effect will give rise to values of $\bar{K}$ of order $+kT$ as found here.

A second explanation for the positive values of $\bar{K}$ that are found is that we may have looked over a term in the size distribution. Now any additional term in the size distribution that is size dependent (e.g. powers or exponentials with j; the first kind of terms arise if the bending elastic moduli are assumed to depend logarithmically on size) will change the shapes of the theoretical curves and therefore ruins the agreement with experiments. This is immediately clear when it is realized that all quantities coupled to the size dependent terms are fixed as shown in Table 1. Therefore the only kind of term that might have been overlooked is one that scales the whole size distribution (or provides a size independent weighting factor), just as $\bar{K}$ does in Eq. (4.3) with (4.4). The physical basis for such a term is however somewhat obscure.

These results stress even more that the detailed expression of the size distribution significantly influences measurable properties of droplet type microemulsions.

6. Final Remarks

In the size distribution for vesicles and microemulsions as derived here, Eq. (4.3 – 4.5), the exponents contain the 'macroscopic' interfacial free energy, i.e. the interfacial area times the second order expansion of the interfacial tension in the inverse radius of the droplets, Eq. (4.2), *without* finite size corrections. The entropic terms, i.e. the terms following from the translational partition function, *and* the finite size effects related to the entropy of the droplet interface, are all in the pre-exponent. This is because they cause a contribution to the free energy that is logarithmic in size. As mentioned before, the pre exponential factor is always determined by the model used. Approaches that are comparable to the one that is taken here all find different pre-exponential factors in the size distribution [8 – 10]. We choose to take a pragmatic approach and estimated the pre-exponential factor from experiments. We emphasize the importance of the use of a physically consistent length scale coupled to translational configurations. With the estimate made in [12], we were able to make a conjecture for the interfacial contribution.

We showed (in Section 3) that microemulsion droplets in equilibrium with excess fluid, or vesicle systems, with positive (macroscopic) interfacial tension, can be stable either due to a factor coupled to interfacial entropy of the droplets or by a preferred curvature with an associated stiffness that leads to a curvature dependence of the interfacial tension. On experimental grounds we ruled out the first possibility. We showed that the experimental trends are indeed consistent with the concept of a curvature dependence of the interfacial tension.

The agreement between theory and experiments is rather good. Not only at a consistency level (where it is actually excellent; Section 5.2), but also when all but one quantities in the theory are fixed. This comparison, however, seems to point to a size independent factor in the size distribution, the physical origin of which is unknown for the time being. We note that a full quantitative test of the theory is possible if e.g. a set of R_w, ϕ, γ data as a function of the salt concentration and the (ionic) surfactant concentration is available, and if the Gaussian bending elastic modulus is obtained, for example, from the full lateral pressure profile of the surfactant monolayer at the oil-water interface [28].

WKK thanks Henk Lekkerkerker and David Morse for discussions on microemulsions and vesicles. This work was supported by the Petroleum Research Fund under grant No. ACS-PRF # 27507-AC9.

References

[1] P.A. Winsor, Trans. Faraday Soc. *44*, 376 (1948).
[2] M. Kotlarchyk and S.H. Chen, J. Chem. Phys. *79*, 2461 (1983).
[3] J. Ricka, M. Borkovec, and U. Hofmeier, J. Chem. Phys. *94*, 8503 (1991).
[4] M. Almgren, R. Johannsson, and J.C. Eriksson, J. Phys. Chem. *97*, 8590 (1993).
[5] W.K. Kegel, I. Bodnàr, and H.N.W. Lekkerkerker, J. Phys. Chem. *99*, 3272 (1995).
[6] S.A. Safran and L.A. Turkevich, Phys. Rev. Lett. *50*, 1930 (1983).
[7] M. Borcovec, Adv. Colloid Interface Sci. *37*, 195 (1992).
[8] M. Borcovec, J. Chem. Phys. *91*, 6268 (1989).
[9] J.C. Eriksson and S. Ljunggren, Progr. Colloid Polym. Sci. *81*, 41 (1990).
[10] J.T.G. Overbeek, Progr. Colloid Polym. Sci. *83*, 1 (1990).
[11] J.T.G. Overbeek, G.J. Verhoeckx, P.L. de Bruyn, and H.N.W. Lekkerkerker, J. Colloid Interface Sci. *119*, 422 (1987).
[12] H. Reiss, W.K. Kegel, and J. Groenewold, J. Ber. Bunsenges. Phys. Chem. *100*, 279 (1996).
[13] J.W. Gibbs, The Scientific Papers of J. Willard Gibbs Volume One: Thermodynam ics; p 252 – 258, Oxbow Press, Woodbridge, Con., 1993.
[14] M. Volmer, Z. Phys. Chem. *125*, 151 (1927).

[15] M.E. Fisher, Physics *3*, 255 (1967).
[16] D.C. Morse and S.T. Milner, To appear in Phys. E.
[17] W. Cai, T.C. Lubensky, P. Nelson, and T. Powers, J. Phys. II (France) *4*, 931 (1994).
[18] R. Aveyard, B.P. Binks, and J. Mead, J. Chem. Soc. Faraday Trans. *82*, 1755 (1986).
[19] G.A. van Aken, Thesis, Utrecht University, The Netherlands (1990).
[20] W. Helfrich, Z. Naturforsch. *28c*, 693 (1973).
[21] W. Helfrich, J. Phys. (France) *46*, 1263 (1985).
[22] L. Peliti and S. Leibler, Phys. Rev. Lett. *57*, 1690 (1985).
[23] F. David, in: Statistical mechanics of membranes and interfaces, ed. by D. Nelson, T. Piran, and S. Weinberg, World Scientific, Singapore, 1989.
[24] B.D. Simons and M.E. Cates, J. Phys. II (France) *2*, 1439 (1992).
[25] M. Gradzielski, D. Langevin, and B. Farago, Preprint.
[26] B.P. Binks, H. Kellay, and J. Meunier, Europhys. Lett. *16*, 53 (1991).
[27] W. Helfrich, in: Les Houches, Session XXXV, 1980, ed. by R. Balian, M. Kléman, J.P. Poirier, Physics of defects, North Holland, Amsterdam, 1981.
[28] I. Szleifer, D. Kramer, A. Ben-Shaul, W.M. Gelbart, and S.A. Safran, J. Chem. Phys. *92*, 6800 (1990).
[29] H.N.W. Lekkerkerker, Phys. A *167*, 384 (1990).
[30] X.-L. Wu, P. Tong, and J.S. Huang, J. Colloid Interface Sci. *148*, 104 (1992).

Presented at the Discussion Meeting of the Deutsche Bunsen-Gesellschaft für Physikalische Chemie "Microemulsions – Experiment and Theory" in Göttingen, September 4th to September 6th, 1995 E 9088